

Impact of KOH Etching on Nanostructure Fabricated by Local Anodic Oxidation Method

Arash Dehzangi^{1*}, Farhad Larki¹, Burhanuddin Y. Majlis^{1*}, Mahmood Goodarz Naseri², Manizheh Navasery², A Makarimi Abdullah³, Sabar D. Hutagalung⁴, Norihan Abdul Hamid¹, Mimiwaty Mohd Noor¹, Mohammadmahdi Vakilian¹ and Elias B. Saion²

¹Institute of Microengineering and Nanoelectronics (IMEN), Universiti Kebangsaan Malaysia, 43600 Bangi, Selangor, Malaysia

²Department of Physics, Faculty of science, Universiti Putra Malaysia, 43400 Serdang, Malaysia

³Advance Material Research Center (SIRIM), Lot 34, Kulim Hi-Tech Park, 09000 Kedah, Malaysia

⁴School of Materials and Mineral Resources Engineering, Universiti Sains Malaysia, 14300 Nibong Tebal, Penang, Malaysia

*E-mail: dehzangi@ukm.my; burhan@vlsi.eng.ukm.my

Received: 3 April 2013 / Accepted: 5 May 2013 / Published: 1 June 2013

In this letter, we investigate the impact of potassium hydroxide (KOH) etching procedure on Silicon nanostructure fabricated by Atomic force microscopy on P-type Silicon-on-insulator. An electrochemical process, as the local anodic oxidation followed by two wet chemical etching steps, KOH etching for silicon removal and hydrofluoric etching for oxide removal, were implemented to fabricate the silicon nanostructures. The effect of the pure KOH concentrations (10% to 30% wt) on the quality of the surface is studied. The influence of etching immersing time in etching of nanostructure and SOI surface are considered as well. Impact of different KOH concentrations mixed with 10% IPA with reaction temperature on etch rate is investigated. The KOH etching process is elaborately optimized by 30% wt. KOH + 10% vol. IPA in appropriate time and temperature. The angle of the walls in etch pit for extracted nanowire reveals some deviation from the standard anisotropic etching.

Keywords: Local anodic oxidation (LAO); Silicon-on-insulator (SOI); potassium hydroxide (KOH) wet chemical etching, isopropyl alcohol (IPA)

1. INTRODUCTION

The conventional techniques for semiconductor fabrication are based on various lithographical methods in top-down approach. Unconventional methods, on the other hand, could provide simpler

ways to achieve nanostructures. Some unconventional methods such as nano-imprint lithography (NIL) [1], soft lithography [2], or atomic force microscopy (AFM) nanolithography [3] can be considered as flexible alternatives for nanoscale patterning and fabrication. Tip induced local anodic oxidation (LAO), as a local oxidation of Si surfaces in air ambient, is one of the most widely investigated processes for AFM nanolithography [4, 5]. This top down fabrication process requires the implementing of Si anisotropic etching.

Different groups reported different wet and dry etching materials and processes. Hydrazine is one of the etchant with the advantage of low degradation during deep etching [6], however extreme precaution is essential since it is highly toxic and potentially explosive. Dry plasma etching methods (e.g. reactive ion etching (RIE)) are another options, which allow to obtain a great variety of etching profiles or aspect ratios. However, the selectivity between the oxide mask and the Si is generally poorer in comparison with liquid etchants [7].

Anisotropic chemical wet etching is still an applicable technique for fabricating simple microstructures and nanostructures on a single crystal silicon on insulator (SOI) wafer. Tetramethyl-amino-hydroxide (TMAH) and potassium hydroxide (KOH) saturated with isopropyl alcohol (IPA) are two well-known etchants which can be used for etching of nanostructures fabricated by LAO technique. However, the TMAH etchant revealed some disadvantage of slow etching rate and a trend to have a rough surface (e.g. hillocks formation) [8, 9]. The most common anisotropic etchant is potassium hydroxide (KOH) which is more recommended compare to other anisotropic etchant (e.g., ethylenediamine, pyrocatechol) for Si etching [10]. The mechanism of KOH anisotropic etching has been elaborately investigated by several teams [11, 12].

In AFM- LAO method, an oxide pattern is transferred on the top Si layer used as a mask for selective etching of the Si. The liquid etching (KOH) attacks uncovered top Si layer, and the desired structure can be extracted by means of selective chemical etching and removal of undesired Si area. KOH etching is known for good silicon/silicondioxide selectivity and its easy performance. The buried oxide layer (BOX) in SOI wafer acts as an etch stop.

The etched structure has a trapezoidal cross section, which is defined by well precise crystalline planes (due to anisotropic etching). This allows an easy reduction of the Si wire dimensions by successive oxidation steps and the regularity of the cross section after the etch, which is an important advantage for the fabrication of small and long nanostructures or nanosensors [13]. Some aspects of the KOH wet etching on nanostructure fabricated by AFM nanolithography have been investigated previously [14], but some impacts of the KOH etching (with or without IPA saturated admixture) like etching time, or reaction time still are interesting issues to be studied. Practically, AFM-LAO oxide (SiO_x) can be an imperfect etch mask due to its fundamental differences, such as structure and electrical properties, with the thermal oxide which may lead to a larger selectivity value [14]. Therefore, the impact of LAO induced mask on the final etched structure can be different in comparison with the thermal oxide mask.

We briefly reported the fabrication of nanodevice by AFM – LAO nanolithography [15, 16] on SOI, using KOH+IPA wet etching [17]. In this work we elaborately investigate the impact of etching process on Si surface and nanoscale devices, as a pure experimental work. The important contributing parameters in etching process like the effect of KOH concentration, reaction temperature or immersing

time of etching on etch rate and surface roughness, are investigated and compared with previous works. In this matter, the specific property of AFM induced oxide was considered on the etched nanostructure. This can use as a guide for future experimental works in AFM nanolithography, KOH etching, and complete the previous ones.

2. METHODOLOGY

LAO was carried out on the p-type B-doped (100) SOI wafer with top Si thickness of 100 nm, buried oxide (BOX) thickness of a 145 nm with a resistivity of 13.5–22.5 Ω cm (Soitech) [18], by using scanning probe microscope machine (SPM) (SPI3800N/4000)[19]. LAO procedure was performed in contact mode employing AFM conductive-coated tips with the force constant of 0.2 N m^{-1} and the resonance frequency of 13 kHz.

The room humidity (RH) was controllable from 50% to 80% with an accuracy of 1%. The oxide growth patterned on SOI top layer (mask), and uncover area was removed by KOH+IPA etching process. Finally, the oxide mask was removed by hydrofluoric acid (HF) in aqueous solution with a well-known ability to dissolve SiO_2 . KOH pellets (molar weight of 56.11 g/mol) are supplied from *System*, Isopropyl alcohol (IPA) (molar weight of 60.10 g/mol) is supplied by *Merck*, and hydrofluoric acid (HF) supplied by JT Baker (concentration of 49 %). The KOH wet etching has significant role in fabrication of nanostructure, with a high rank of accuracy and precaution. All KOH etching experiments were carried out in a closed glass beaker with a constant temperature bath, stirred in order to get uniform etching rate. The structure has a simple shape consists of the square pads (as the contacts) and a nanowire between the pads as a channel [15]. The morphology of the etched surfaces was also observed using scanning electron microscopes (SEM) (HITACHI 4300 and JEOL JSM-6360). The surface profiler instrument (Tencor P-12, Sitek System) used for surface roughness measurement.

3. RESULTS AND DISCUSSION

In order to study KOH impact on surface of the wafer, some p-type (100) Si samples were exposed by KOH at different concentrations. Figure 1 shows AFM micrograph images of the etched Si wafer for different KOH percentage in solution (10-30%wt) at the range of temperature between 63-65°C (optimized temperature for fabrication). It can be seen that the surface roughness changes as the percentage of KOH increases from 10%wt up to 30% wt. For low percentage of KOH the surfaces is rougher and the formation of insoluble precipitates are more visible. Similar observations are reported in previous works in KOH wet etching [20, 21]. Although the concentration alone is not the main factor on surface roughness, temperature and etching time are also contributing in this matter.

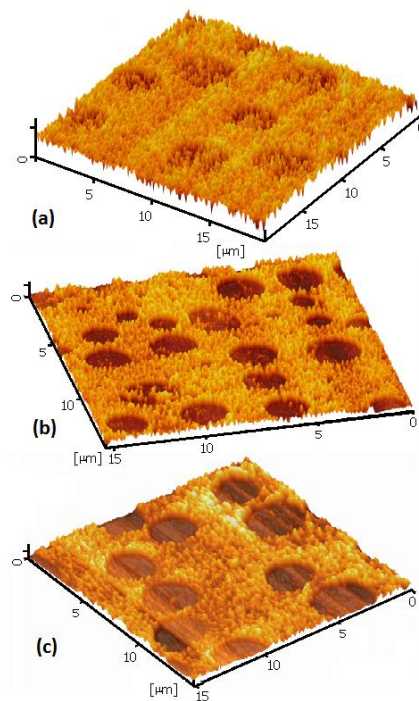


Figure 1. AFM Micrograph images of the SOI surface etched with KOH: (a) 10% wt (b) 20% wt (c) 30% wt

Figure 2, illustrates the relationship between the surface roughness and the temperature at various KOH concentration percentage for p-type (100) Si samples. The graph reveals that the surface roughness, after etching by different KOH concentrations, increases with the temperature up to the highest value at the temperature of 75°C, and the smoother Si surface is achievable at higher concentration of KOH.

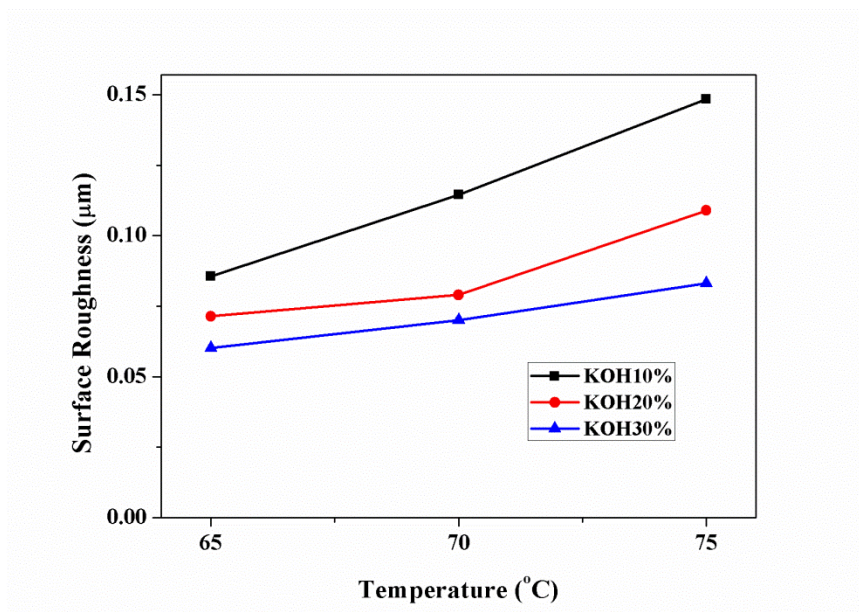


Figure 2. Effect of the reaction temperature on the surface roughness at different KOH concentrations

In reported cases, the etching temperature was normally taken between 55°C-70°C to reach acceptable edge cutting for patterned nanostructure [10]. The etch rate and concentration of KOH has lowest dependence at the temperature below 70°C, and faster etch rate can be achieved by using a high-temperature reaction [10, 22]. The time of etching or immersing time depends on thickness of Si in SOI, which is desired to be removed. In our case, since the rate of Si removal for KOH etching is assumed to be 0.25 $\mu\text{m}/\text{min}$ [23], time interval estimation for removing of 100 nm of the top Si layer is between 20-22 s.

Figure 3 shows the effect of immersing time on the nanostructure after KOH (30%wt) etching process at the temperature range of 63°C- 65°C. This KOH concentration is taken according to the optimized parameters reported previously [15]. As we can see the best shape extracted after 20s (Figure3a) of etching, while for longer immersing time (25-30s) the over etching is appeared and some parts of the structure are removed. However, surface roughness is higher for shorter immersing time (20s) compare to the other times. The same effect are reported in [10, 24].

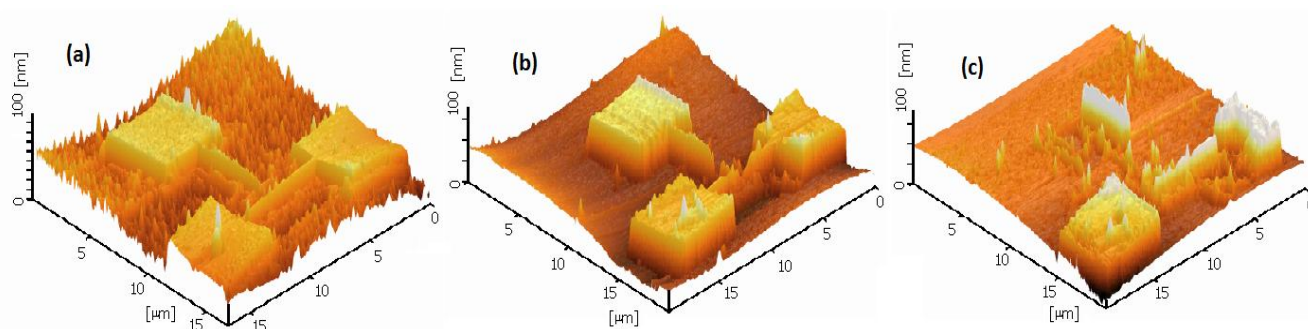


Figure 3. AFM image of nanostructure after etching by KOH 30%wt. for different immersing time, a) 20 s, b) 25 s, and c) 30 s

During the KOH etching process, hydrogen bubbles are producing due to reaction of Si and the hydrogen ion. These bubbles may act as a surface mask against the reaction sites [25, 26]. The number of bubbles is directly proportional to the temperature, whereas the size of the bubbles is reversely related to the etchant concentration. On the other hand, the sharpness of the etched structure is important in fabrication of nanodevices, which requires monitoring the temperature and KOH concentration together. In the KOH etching process, it was observed that by increasing the KOH concentration the density of bubbles increased but the size of the bubbles decreased, the same effect already has been reported [10]. In fact, an admixture of isopropyl alcohol (IPA) in KOH etchant can improve the smoothness of the surface after etching[27].The influence of the IPA admixture in KOH etching was elaborately investigated in reported cases [10, 26].

Addition of IPA improves the surface roughness due to the increased wettability of the resulting etchant. This process reduces the stability of hydrogen bubbles (tensioactive character).The etching rate strongly depends on water concentration, and water content in solution extremely decreases with the high KOH concentration[28]. Adding IPA can liberate water particles in the close vicinity of Si surface by hindering hydration of K^+ and OH^- ions [27]. This mechanism prevents the

formation of pyramidal hillocks, which known as the most common reasons for having a higher surface roughness of the $\langle 100 \rangle$ Si [29]. The presence of IPA interrupts the access of OH^- ions across the surface and reduces the oxidation rate. This provides an equilibrium in diffusion and oxidation of reaction products and decreases the duration of the attached hydrogen bubbles to the etched surface, which leads to have more smoothness of the surface [8, 11]. It is important to mention that using IPA addition may reduce the etching rate but it definitely provides smooth (100) Si surface in the whole range of examined concentration of KOH, specially for a high KOH ratio [30].

The effect of the IPA concentration on KOH etching rate for Si (100) is shown in Figure 4, at different temperatures ($60\text{--}63^\circ\text{C}$) for different KOH concentrations (10%–50%). It shows decrement of etching rate by increasing the IPA concentration with the lowest etch rate for the KOH concentration of 50%wt in all examined IPA concentrations. At this rate of KOH concentration (50%wt), the lowest dependence of the etch rate with IPA% variation was observed. It must be mentioned that the 50% of IPA in KOH solution provides an unstable condition during the etching, considering the alcohol evaporation and difficult saturation, due to the high rate of IPA in solution. The highest etching rate was achieved at 10% of IPA admixture for all examined KOH concentration. The results show that the etch rate decreases with increasing the KOH concentration at constant temperature, which is in agreement with previous works [10, 27].

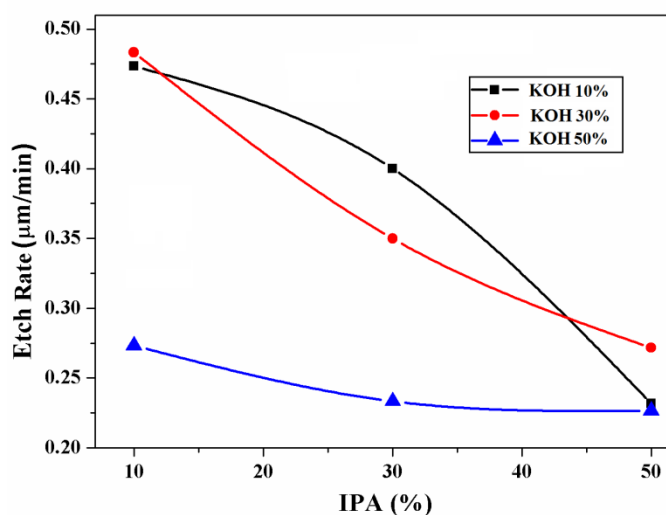
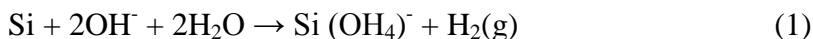


Figure 4. Etching rate of Si (100) for KOH mixed with different IPA %vol. at 60 C°

For different temperatures, the impact of the different KOH concentrations on etch rate was examined for the solutions mixed with 10% of IPA, as it is shown in Figure 5. Regardless of the etch sharpness or surface roughness, it was observed that the fastest etch rate can be achieved by using a high-temperature reaction. However, high temperature ($>80\text{ }^\circ\text{C}$) procedure has destructive effect on the thin Si layer in SOI sample (as in our case), which leads to have uneven or twisted surface.

The graph shown in Figure 5 indicates that the variation of the etch rate with KOH concentration has minimal dependence at lower temperatures (like $50\text{ }^\circ\text{C}$ and $60\text{ }^\circ\text{C}$) in comparison with the higher one ($70\text{ }^\circ\text{C}$). Furthermore, it shows that the etch rate increases with increasing reaction

temperature, for all examined range of KOH concentrations. At 60 °C and 70 °C, a maximum etching rate is obtained for 30wt % KOH + 10% of IPA. The variation in etch rate for these two reaction temperatures shows, first, an increase with KOH concentration up to 30%wt and then a decrease for more increasing of the KOH concentration up to 50%wt. The reason can be explained by considering the Si etching reaction. In general, the etching process in order to remove the Si in KOH solution is expressed by the following reaction:



When KOH reacts with Si, soluble $\text{Si}(\text{OH})_4^-$ with H_2 (Hydrogen bubbles) will be formed. At a low KOH concentration, OH^- ions are in low concentration, whereas the numbers of H_2O molecules are low at high KOH concentration. Accordingly, the reaction can be slow down at high and low KOH concentrations. However, the precise extracted rates or concentrations can be affected by different IPA percentage in admixture.

As a conclusion, it can be said that the etching temperature has much more significant effect on etch rate than changing KOH concentration, in the range of examined temperature ($\leq 70^\circ\text{C}$). Yun [10] reported the same result for the etch rate of KOH admixture with 10% of IPA. It is worth noting that for pure KOH etchant, the best etch rate appears at lower KOH concentration [12, 27].

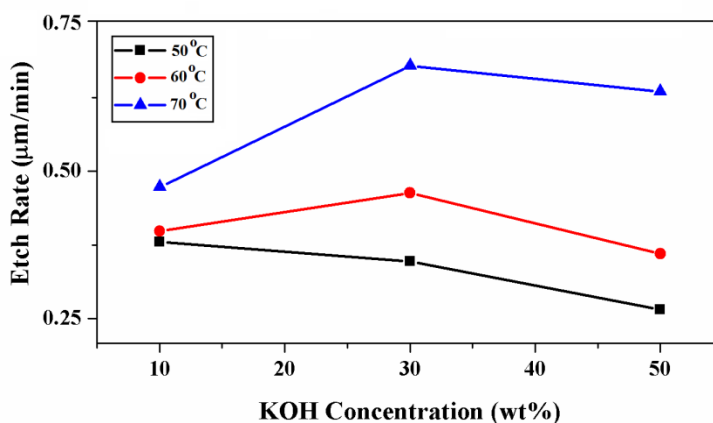


Figure 5. Etching rate of Si (100) for different KOH mixed with IPA (10% vol)

The effect of the KOH concentration mixed with IPA on quality of the etching surface for nanostructure was examined [19, 31]; by the higher KOH concentration (40%wt KOH + 10%vol IPA), the structure was over-etched with lower rate of sharpness after etching process. Based on our experiment and the related literature [10,17, 26], the etchant solution of 30%wt KOH + 10%vol. IPA was optimized.

The role of immersing time and temperature were also considered in obtaining the optimum result for nanostructure formation with a proper surface roughness. In anisotropic etching for (100) Si, the etch pit have a pyramid shape, and walls are flat and angled [10, 27]. Regarding to literature, the etching will be stopped at (111) plane wall at an angle of 54.7° [32]. For KOH etching, the etch rate for high index planes, e.g. (411), (311) or (211), grows faster than low index plane, like (110) or (111) [27, 33]. At the shorter immersing time, high index planes of the Si surface are more etched compare to the

lower index planes, and then the pit walls are less angled compare to the case of longer immersing time. In Figure 6 (a,b), AFM images of the structure before and after etching are shown. In this case, after 10 seconds of etching, the structure is under-etched with the broadened edges.

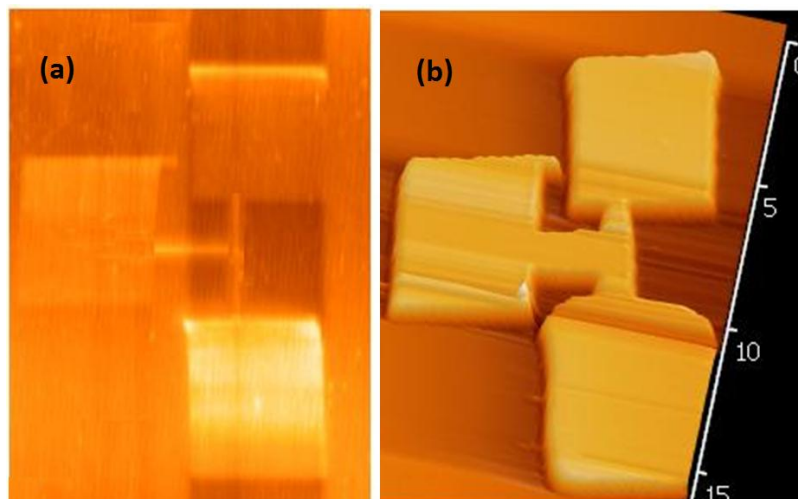


Figure 6. AFM topography images of the structure, a) after LAO and b) after etching process (under etched) with the solution of 30% wt. KOH + 10% IPA at 63°C, after 10 seconds immersing time

It can be interesting to examine the effect of etching time of the optimized etching solution on SOI surface. The whole process of Si etching process can approximately be split up into three major procedures. First, the infusion of the etchant on the boundary layer that leads to etchant diffusion across the surface of the wafer; then the etchant chemical reaction begins with the Si atoms located at the surface, and finally the diffusion of this chemical reaction spreads through to the bulk [8]. Which in our case, for SOI wafer with a thin top Si layer and short etching time (< 25 s), the third procedure, as the reaction progress from the etched surface to the bulk etchant [34], cannot be occurred completely. Figure 7(a-c) demonstrate SEM image comparison for the effect of the etching time variation on the SOI surface after etched by 30%wt KOH + 10%vol. IPA at 5s, 10s and 20s respectively. It shows that how the etchant influences the SOI surface during the etchant diffusion across the surface, which leads to beginning of the chemical reaction. This provides increasing of the surface roughness, when the time of etching is increased up to 20s. During the etching process, the transport velocity of the fresh etchant toward the silicon wafer, as a significant factor that can affect the etch rate, is determined by the gradient of the etchant concentration. It is important to mention that reaction velocity of the etchant and Si atoms are mainly related to the etching temperature, etchant concentration and additives [34].

The optimized range of etching temperature for the best smoothness and sharpness was achieved at 63-65 °C, when the etching time was adjusted for 20s to 22s. Lower range of temperature may enhance the absorption of IPA on Si surface, which blocks the effect of IPA. The solution was stirred at 600 rpm (to have uniform etching in all directions) and the substrate was rinsed by deionized water (DIW) for a few seconds after etching.

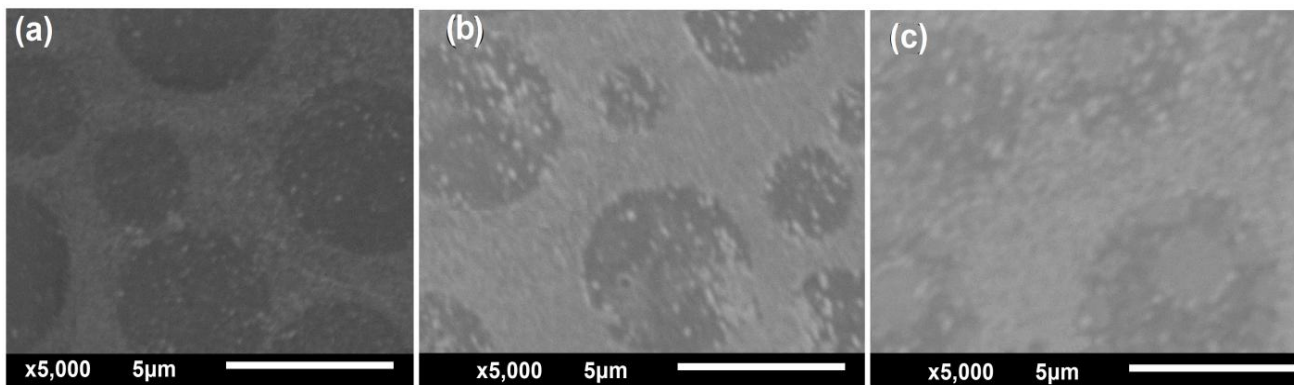


Figure 7. SEM images of the effect of 30%wt KOH + 10% vol. IPA etching time on the SOI surface after a) 5s, b) 10s, c) 20s

After KOH etching, the samples are etched with diluted hydrofluoric acid (H₂O/HF 100:1) at room temperature for 12-14 seconds (stirred at 600 rpm) to remove the SiO₂ mask. This short time period is enough to remove the thin oxide mask (3-4 nm) [15] and native oxide. It is worth mentioning that some parts of the mask was already removed during the anisotropic etching process. Figure 8 demonstrates the AFM image and profile images of the structure after etching process for optimized parameters. As it can be seen in AFM profile image (top), all top Si layer of SOI (100 nm) has been removed.

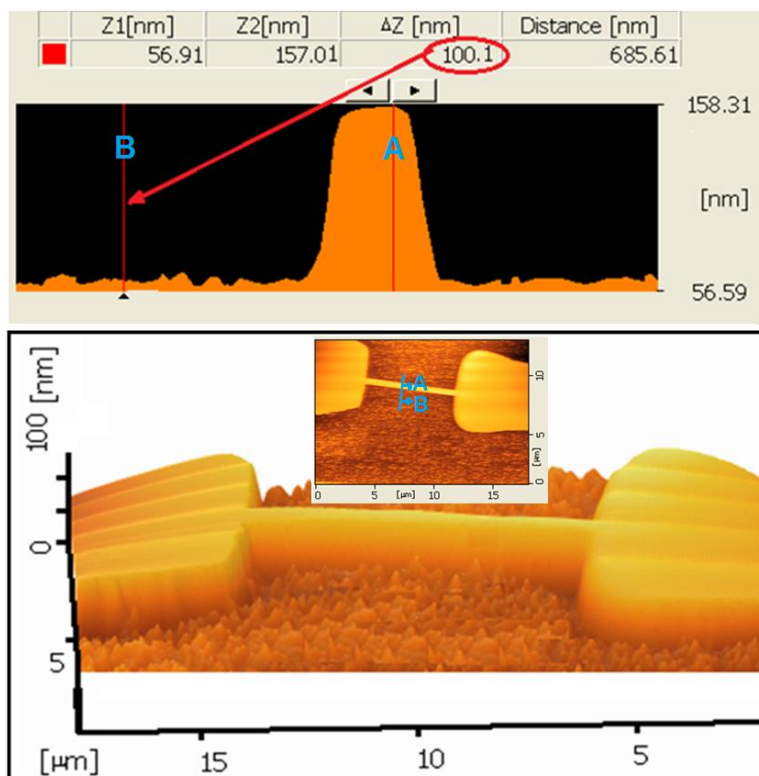


Figure 8. AFM profile image of the nanowire (top) and AFM images of the nanostructure after etched by 30%wt KOH + 10% vol. IPA at 63 - 65 °C

Energy dispersive x-Ray (EDX) analysis and SEM image of the structure after KOH etching and mask removal are shown in Figure 9. For the pointed area on the structure surface (Figure 9a), the EDX analysis indicated that the atomic element contained 72.30 % silicon (Si) and 27.70 % oxygen (O). The same analysis for out of the structure area (Figure 9a) revealed that the selected area contained 63.75 % oxygen (O) and 36.25% silicon (Si). During HF etching, the oxide mask and the native oxide are expected to be removed. Therefore the structure should contain a small amount of oxygen (O). However, the existence of oxygen on the Si structure area (Figure 9a) may originate from the underlying BOX layer. The volume of the electron penetration in the sample contributes to the element percentage results. For the energy range of the primary electron used in EDX analysis (5.0 kV), the depth penetration for the SiO₂ is 0.253 μ m by calculation with Kanaya-Okayama depth penetration formula [35]. The sample thickness is only \sim 0.100 μ m, so the results cannot show clearly the exact percentage. By the way, the results still show the acceptable difference between the Si and O atomic percentage.

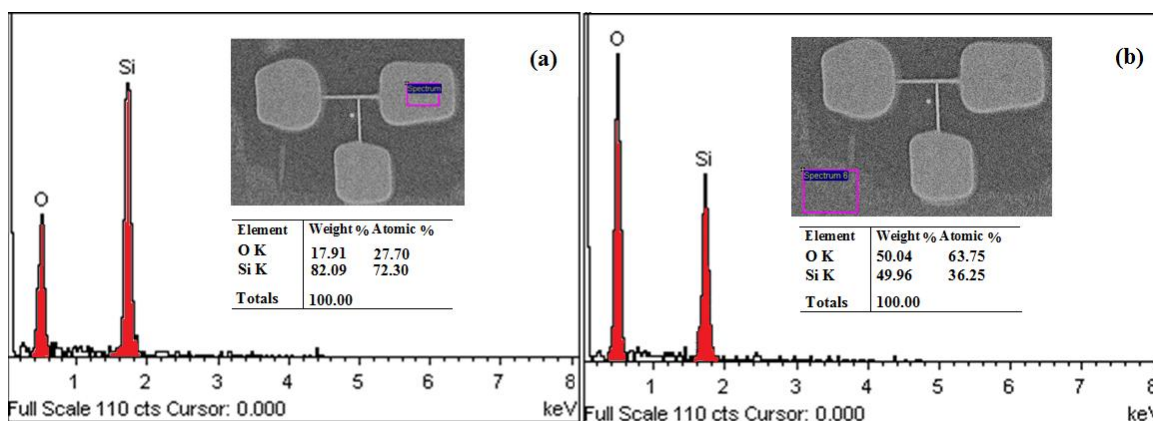


Figure 9. EDX analysis of the Si nanostructure after etching processes measured, a) on the structure, b) out of the structure area on BOX

Figure 10 shows the high magnification transmission electron microscopy (TEM) image of the nanowire profile for an arbitrary sample after anisotropic etching with KOH 30%wt. + 10% vol. IPA and HF etching processes (oxide removal). It shows pyramid shape profile for the nanowire with flat and angled walls. According to the size measurement by TEM instrument, the angle of the etched structure is found 51.97° (Figure 10), which is smaller than reported cases for the standard Si anisotropic etching (54.74°) [10]. The reason can be studied by considering that the etching rate in (111) plane is not completely stopped. For (100) plane during the etching process, two dangling bond is exposed by the etchants (i.e. hydroxide ions), whereas for the case of a (111) plane, only one dangling bond is exposed to the etching solution [10]. Accordingly, etching in the (111) plane would be more slowly than in the (100) plane, but it is not completely stopped, and the angle can be smaller than 54.74° for standard (111) plane.

Another reason for the angle difference may come from the poorer quality of the oxide layer in LAO compare to the annealed oxide. It is known that the properties of the non-annealed oxide created

by AFM-LAO are different from the thermally grown oxide. Un-annealed anodic oxides have the lower density of 2.05 vs 2.27 (g cm^{-3}), the higher dielectric constant of 5.2 vs 3.9 [36], and the greater H_2O content of ~4%–5% by weigh [37], in comparison with thermally grown oxide respectively. According to the different quality and thickness of the grown oxide by LAO, for etching procedure the selectivity of etchant is a critical parameter to achieve a high aspect ratio for nanostructures. As far as the etching selectivity is concerned for experimental works, low selectivity of silicon/silicon dioxide for AFM-LAO is another issue for the etching process. In fact, for KOH solution, a silicon/AFM-LAO pattern etching selectivity value of 40:1 has been reported [38]. This low selectivity may provide higher undercutting of the both Si and oxide mask, especially at the edge of the oxide layer due to the poorer quality.

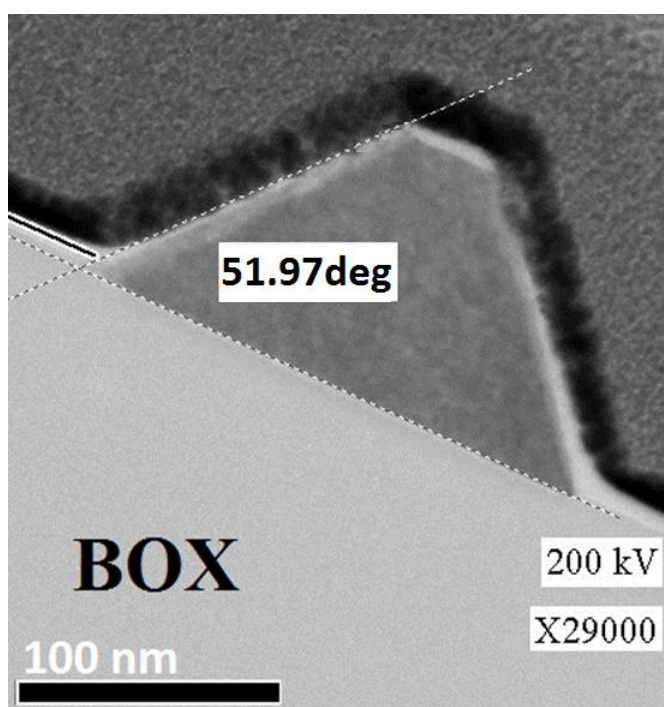


Figure 10. TEM micrograph of nanowire after etching process (modified from [15])

The reduction of the structure width after KOH etching is another cause needed to be considered. This effect is likely because of the imperfect etch mask. An inhomogeneous local electric field at the AFM tip, during the oxidation, leads to a lower quality (e.g. formation of non-uniformity) across the oxide (SiO_x) mask [14].

In Table 1, we reported the height of the LAO induced oxide and the etching depth for different samples. For oxide height greater than 2 nm, the heights of the etched Si are nearly constant. Small variations of the etching depth can be explained due to the existence of oxide patterns (with different height) on the top of the etched Si which can make some variations of the Si heights after etching. On the other hand, the oxide patterns smaller than 1.5 nm make significant decrease in height of Si structure after etching, and the oxide height less than 1 nm cannot bring about any remarkable Si

structure after etching. The same trend reported for AFM-LAO (for tapping mode) in [39]. It is worth to mention that for high KOH concentration used in this study, the whole patterned oxide and underneath Si disappeared for thin oxide layer (<1.5 nm).

Table 1. Heights of the oxide patterns and resulting silicon structure after etching

Sample No.	1	2	3	4	5	6
Oxide height (nm)	3.1	2.9	2.5	2	1.5	1
Etching depth(nm)	100	99.1	99	87	45	~ 0

4. CONCLUSION

Simple nanostructures were fabricated on SOI by AFM-LAO nanolithography. KOH wet etching processes were optimized to extract the structure after LAO process, and then the HF etching for Silicon oxide removal was used. The optimized condition is the solution of 30%wt. KOH with 10%vol. IPA for wet etching at 63°C reaction temperature, 20 seconds for immersing time stirred at 600rpm. The impact of the parameter variation, such as different KOH concentrations with or without IPA admixture, different etching immersing time, and reaction temperature on the structure or the Si surface were investigated. For the nanowire profile, the angle of the wall in etching pit after etching was 51.97°.

ACKNOWLEDGEMENTS

The authors gratefully acknowledge that this work was financially supported by Universiti Kebangsaan Malaysia through the grant project “NANOELEKTRONIK DAN MEMS SENSOR” with the code of “DIP-2012-16”, and USM RU Grant no. 1001/PBAHAN/814167.

References

1. L. J. Guo, *Advanced Materials*, 19 (2007) 495-513.
2. D. Qin, Y. Xia, and G. M. Whitesides, *Nature protocols*, 5 (2010) 491-502.
3. Y. Zhang, S. Santhanam, J. Liu, and G. Fedder, "Active CMOS-MEMS AFM-like conductive probes for field-emission assisted nano-scale fabrication", (2010) 336-339.
4. F. Larki, S. D. Hutagalung, A. Dehhangi, E. Saion, A. Abedini, A. M. Abdullah, M. Hamidon, and J. Hassan, *Microelectronics and Solid State Electronics*, 1 (2012) 15-20.
5. M. Tello, *Applied Physics Letters*, 79 (2001) 424-426.
6. Y. K. Choi, D. Ha, T. J. King, and J. Bokor, *Japanese journal of applied physics* 42 (2003) 2073-2076.
7. H. Jansen, H. Gardeniers, M. Boer, M. Elwenspoek, and J. Fluitman, *Journal of Micromechanics and Microengineering*, 6 (1996) 14.
8. C. R. Yang, P. Y. Chen, C. H. Yang, Y. C. Chiou, and R. T. Lee, *Sensors and Actuators A: Physical*, 119 (2005) 271-281.

9. L. M. Landsberger, S. Naseh, M. Kahrizi, and M. Paranjape, *Microelectromechanical Systems, Journal of*, 5 (1996) 106-116.
10. M. Yun, *Journal-Korean physical society*, 37 (2000) 605-610.
11. H. G. G. Philipsen and J. J. Kelly, *Electrochimica acta*, 54 (2009) 3526-3531.
12. I. Zubel, I. Barycka, K. Kotowska, and M. Kramkowska, *Sensors and Actuators A: Physical*, 87 (2001) 163-171.
13. G. Pennelli and M. Piotto, *Journal of applied physics*, 100 (2006) 054507-054507-9.
14. F.-S. Chien, C.-L. Wu, Y.-C. Chou, T. Chen, S. Gwo, and W.-F. Hsieh, *Applied Physics Letters*, 75 (1999) 2429-2431.
15. A. Dehzangi, A. M. Abdullah, F. Larki, S. D. Hutagalung, E. B. Saion, M. M. N. Hamidon, J. Hassan, and Y. Gharayebi, *Nanoscale research letters*, 7 (2012) 381.
16. A. Dehzangi, F. Larki, E. Saion, S. D. Hutagalung, M. Hamidon, and J. Hassan, "Field effect in silicon nanostructure fabricated by Atomic Force Microscopy nano lithography", in IEEE Regional Symposium on Micro and Nanoelectronics (RSM), Kota Kinabalu (2011) 104-107.
17. F. Larki, A. Dehzangi, A. Abedini, A. M. Abdullah, E. Saion, S. D. Hutagalung, M. N. Hamidon, and J. Hassan, *Beilstein J. Nanotechnol*, 3 (2012) 817-823.
18. SOITEC. PTF, 38190 Bernin France [Online]. Available: <http://www.soitec.com/en/index.php>
19. A. Dehzangi, F. Larki, S. Hutagalung, E. Saion, A. Abdullah, M. Hamidon, B. Majlis, S. Kakooei, M. Navaseri, and A. Kharazmi, *Micro & Nano Letters, IET*, 7 (2012) 981-985.
20. S. Youn and C. Kang, *Wear*, 261 (2006) 328-337.
21. G. Pennelli, M. Piotto, and G. Barillaro, *Microelectronic engineering*, 83 (2006) 1710-1713.
22. K. Biswas and S. Kal, *Microelectronics journal*, 37 (2006) 519-525.
23. H. Seidel, L. Csepregi, A. Heuberger, and H. Baumgartel, *J. Electrochem. Soc*, 137 (1990) 3612-3625.
24. W. Haiss, P. Raisch, L. Bitsch, R. J. Nichols, X. Xia, J. J. Kelly, and D. J. Schiffrin, *Journal of Electroanalytical Chemistry*, 597 (2006) 1-12.
25. H. Camon and Z. Moktadir, *Microelectronics journal*, 28 (1997) 509-517.
26. I. Zubel and M. Kramkowska, *Sensors and Actuators A: Physical*, 101 (2002) 255-261.
27. I. Zubel and M. Kramkowska, *Sensors and Actuators A: Physical*, 93 (2001) 138-147.
28. H. Seidel, L. Csepregi, A. Heuberger, and H. Baumgärtel, *Journal of the Electrochemical Society*, 137 (1990) 3612-3626.
29. I. Zubel and M. Kramkowska, *Sensors and Actuators A: Physical*, 115 (2004) 549-556.
30. A. Merlos, M. Acero, M. Bao, J. Bausells, and J. Esteve, *Sensors and Actuators A: Physical*, 37 (1993) 737-743.
31. A. Dehzangi, F. Larki, J. Hassan, S. D. Hutagalung, E. B. Saion, M. N. Hamidon, A. M. Abdullah, A. Kharazmi, S. Mohammadi, and B. Y. Majlis, *Nano Hybrids*, 3 (2013) 93-113
32. V. Lindroos, M. Tilli, A. Lehto, and T. Motooka, *Handbook of silicon based MEMS materials and technologies: William Andrew*(2009).
33. C. Ju and P. J. Hesketh, *Thin solid films*, 215 (1992) 58-64.
34. C.-R. Yang, P.-Y. Chen, C.-H. Yang, Y.-C. Chiou, and R.-T. Lee, *Sensors and Actuators A: Physical*, 119 (2005) 271-281.
35. K. Kanaya and S. Okayama, *Journal of Physics D: Applied Physics*, 5 (2002) 43.
36. P. Schmuki, H. Böhni, and J. Bardwell, *Journal of the Electrochemical Society*, 142 (1995) 1705.
37. P. Yang, W. Lau, S. W. Lai, V. Lo, S. Siah, and L. Chan,
38. J. Dagata, T. Inoue, J. Itoh, K. Matsumoto, and H. Yokoyama, *Journal of applied physics*, 84 (1998) 6891-6900.
39. B. Legrand, D. Deresmes, and D. Stievenard, *Journal of Vacuum Science & Technology B: Microelectronics and Nanometer Structures*, 20 (2002) 862-870.